

# Optical Control of the Thermal Conductivity in BaTiO<sub>3</sub>

Claudio Cazorla, Carlos Escorihuela-Sayalero, Jesús Carrete, Jorge Íñiguez-González, and Riccardo Rurali\*

Achieving dynamic control over thermal conductivity remains a formidable challenge in condensed matter physics and materials science, particularly due to the limitations of traditional approaches like structural modifications and doping, which yield static and often irreversible effects. In this study, a solution is demonstrated to this conundrum through light-driven manipulation of thermal conductivity in the archetypal ferroelectric BaTiO<sub>3</sub> (BTO). We analyze, using first-principles simulations, how photoinduced charge injection triggers a ferro-to-paraelectric phase transition, yielding ultrafast, reversible changes in thermal transport properties. These results reveal a substantial reduction in lattice thermal conductivity, especially at low photoexcited charge densities, as the material undergoes a polar-to-nonpolar transformation. This reduction is primarily due to the suppression of low-frequency phonon modes, which limits heat flow as a result of enhanced phonon–phonon scattering. These findings underscore a step forward in tunable thermal conductivity, offering new prospects for efficient thermal management in advanced electronics and energy-harvesting applications.

Typically,  $\kappa$  tuning is realized through the introduction of structural defects and nanostructuring<sup>[5]</sup> in materials. However, these modifications are static and irreversible and the thermal conductivity can only be reduced. The possibility of dynamically tuning  $\kappa$ , on the other hand, would allow for more sophisticated manipulations of the materials thermal properties, paving the way to, for instance, selective cooling of hot spots and the design of thermoelectric modules with adjustable figures of merit or heat scavengers compliant with varying environmental conditions.

In polar (magnetic) materials, external electric (magnetic) fields can be used to trigger phase transitions that potentially are accompanied by sizable  $\kappa$  changes.<sup>[6–8]</sup> These transitions are reversible and fast, thus extremely promising.<sup>[9]</sup> In ferroelectric oxides, electric fields can be used to write/erase domain walls<sup>[10–14]</sup> and trigger nonpolar  $\rightarrow$  polar phase transitions.<sup>[6,15]</sup> However, field-induced polar  $\rightarrow$  nonpolar phase transition normally are not possible: an electric polarization,  $P$ , can be reoriented<sup>[16]</sup> or switched<sup>[17–19]</sup> by an electric bias, but not suppressed.

The nonpolar (or paraelectric) phase of a ferroelectric becomes thermodynamically stable above a particular critical temperature,  $T_c$ . However, using temperature to dynamically control  $\kappa$  is not practical: (i) it limits the applicability range to temperatures that typically are above room conditions (e.g., 760 K for PbTiO<sub>3</sub> and

## 1. Introduction

The design of materials with tailor-made thermal conductivity,  $\kappa$ , can be considered as a pressing challenge in condensed matter physics and materials science owing to its many potential repercussions in modern electronics<sup>[1]</sup> and thermoelectric energy harvesting.<sup>[2]</sup> In one case, high- $\kappa$  materials are necessary to minimize thermal loads in micro/nanoelectronic integrated circuits;<sup>[3]</sup> in the other, high thermoelectric performances are only achievable through low thermal conductivities.<sup>[4]</sup>

C. Cazorla, C. Escorihuela-Sayalero  
Departament de Física, Universitat Politècnica de Catalunya  
Campus Diagonal-Besòs  
Av. Eduard Maristany 10–14, Barcelona 08019, Spain

C. Cazorla, C. Escorihuela-Sayalero  
Research Center in Multiscale Science and Engineering  
Universitat Politècnica de Catalunya, Campus Diagonal-Besòs  
Av. Eduard Maristany 10–14, Barcelona 08019, Spain

J. Carrete  
Instituto de Nanociencia y Materiales de Aragón (INMA)  
CSIC-Universidad de Zaragoza  
Zaragoza 50009, Spain

J. Íñiguez-González  
Luxembourg Institute of Science and Technology (LIST)  
Avenue des Hauts-Fourneaux 5, Esch/Alzette L-4362, Luxembourg

J. Íñiguez-González  
Department of Physics and Materials Science  
University of Luxembourg  
41 Rue du Brill, Belvaux L-4422, Luxembourg

R. Rurali  
Institut de Ciència de Materials de Barcelona  
ICMAB–CSIC  
Campus UAB, Bellaterra 08193, Spain  
E-mail: rrurali@icmab.es

The ORCID identification number(s) for the author(s) of this article can be found under <https://doi.org/10.1002/adfm.202425424>

© 2025 The Author(s). Advanced Functional Materials published by Wiley-VCH GmbH. This is an open access article under the terms of the [Creative Commons Attribution-NonCommercial-NoDerivs License](#), which permits use and distribution in any medium, provided the original work is properly cited, the use is non-commercial and no modifications or adaptations are made.

DOI: 10.1002/adfm.202425424

420 K and for BaTiO<sub>3</sub>); (ii) temperature changes are slow and energy intensive, hence not suitable for technological applications.

An appealing alternative to thermal and electric  $\kappa$  control in polar materials is offered by photoinduced phase transitions (PIPT), where photoexcited carriers screen the long range dipolar interactions and thus may suppress polar order.<sup>[20–22]</sup> An important advantage of PIPT, besides being potentially ultrafast and reversible, is that they may occur over a wide range of ambient temperatures defined by the condition  $T < T_c$ : as far as the material is in a polar state at *dark* conditions, photoabsorption can transform it into a nonpolar state. A similar PIPT phase transition has been recently demonstrated in 2D materials with a charge density wave (CDW) instability,<sup>[23,24]</sup> and the implication for thermal transport have been discussed in the case of TiSe<sub>2</sub>.<sup>[25]</sup> PIPT in ferroelectrics can also be exploited to stabilize different types of topological phonons<sup>[21]</sup> and engineer giant photocaloric effects.<sup>[26]</sup>

In this study, we theoretically analyze with first-principles calculations the polar  $\rightarrow$  nonpolar PIPT in the prototypical lead-free ferroelectric perovskite BaTiO<sub>3</sub> (BTO) (experimentally reported, e.g., in Refs. [27–29]), focusing on the effects on thermal transport and quantifying the changes in the lattice thermal conductivity. A nontrivial relationship between photoinduced carriers and  $\kappa$  modification is revealed. In particular, we find that the largest thermal conductivity changes are obtained for photoexcited charge densities that are close to the minimum threshold necessary for stabilizing the nonpolar phase. This behavior is traced back to the role of the soft mode in the anharmonic scattering rate of low-frequency heat-carrying phonons.

## 2. Computational Methods

### 2.1. Thermal Conductivity Calculations

Density-functional theory (DFT) calculations were performed with the Vienna Ab initio Simulation Package (VASP),<sup>[30–32]</sup> using an energy cutoff of 650 eV, the projector augmented wave method,<sup>[33]</sup> and the generalized-gradient approximation (GGA-PBEsol<sup>[34]</sup>). We treated as valence the following electrons: Ba 6s<sup>2</sup> 5p<sup>6</sup> 5s<sup>2</sup>, Ti 3d<sup>4</sup> 4s<sup>2</sup> 3p<sup>6</sup>, and O 2s<sup>2</sup> 2p<sup>4</sup>. The Brillouin zone corresponding to the 5-atom elemental perovskite cell was sampled with a 12  $\times$  12  $\times$  12 **k**-points grid and the atomic positions were optimized until all the atomic forces were smaller than 0.005 eV/Å.

We computed second-order harmonic interatomic force constants (IFCs) by finite differences in 3  $\times$  3  $\times$  3 supercells, generating the minimum set of nonequivalent displacements with the Phonopy package.<sup>[35]</sup> Finite temperature, renormalized phonons were calculated with the DynaPhoPy code<sup>[36]</sup> by carrying out a normal-mode decomposition from ab initio molecular dynamics (AIMD) simulations. Long AIMD simulations of about 100 ps were carried out in the NVT ensemble using 3  $\times$  3  $\times$  3 supercells. Anharmonic IFCs were calculated also for 3  $\times$  3  $\times$  3 supercells with the help of thirddorder.py.<sup>[37]</sup> We considered three-phonon processes, neglecting interactions beyond 4 Å (6 Å) for the tetragonal (cubic) phase (see the Supporting Information for convergence test of this parameter).

The harmonic and anharmonic IFCs are then used as inputs to solve the phonon Boltzmann Transport Equation (BTE) beyond

the Relaxation Time Approximation (RTA) with the almaBTE code<sup>[38]</sup> on a 26  $\times$  26  $\times$  26 **q**-point grid (convergence tests are reported in the Supporting Information). Non-analytical corrections have been included in the calculation of  $\kappa$  in the absence of photoexcited charges. These computational parameters yield a room temperature thermal conductivity of tetragonal BTO in very good agreement with experimental measurements.<sup>[19]</sup>

Thermal expansion effects were taken into account at zero pressure using the quasi-harmonic approximation (QHA).<sup>[8,39,40]</sup> To this end, we computed the Kohn–Sham and vibrational free energies of the two involved phases considering five different volumes, the smallest of which corresponds to the equilibrium volume at zero temperature. For each volume, the lattice vectors were adjusted so that the value of the off-diagonal strain–stress tensor components were all null and the three diagonal components equal. The Kohn–Sham energies were interpolated as a function of volume using a Birch–Murnaghan equation of state, while the vibrational free energies were interpolated using polynomials of the volume at room temperature.

### 2.2. Photoexcited States

In this work, we describe stationary excited states (under constant illumination) by tuning the smearing of the Fermi–Dirac electronic occupation distribution in the DFT calculations. Similarly to the  $\Delta$ SCF or quasi-Fermi level methods,<sup>[21,41,44]</sup> a fraction of the electronic occupation is redistributed from valence to conduction states according to a Fermi distribution with increased smearing. This simplified approach speeds up considerably the convergence of the electron density in large supercells, such as those required in the present study, while providing an effective description of the lattice relaxation in the presence of excited charges. Noteworthy, in the particular case of photo-induced suppression of ferroelectricity in perovskite oxides, Paillard and coworkers<sup>[20]</sup> explicitly showed that electronic smearing correctly reproduces the results obtained with the more versatile quasi-Fermi level method.

## 3. Results and Discussion

### 3.1. Photoinduced Polar $\rightarrow$ Nonpolar Phase Transition

At room temperature, BTO has a tetragonal structure, with space group *P4mm*, and is ferroelectric. We obtained the lattice parameters  $a = b = 3.969$  Å (short-axis) and  $c = 4.065$  Å (long-axis), and an electric polarization  $P = 30.8$   $\mu\text{C cm}^{-2}$ , which are in good agreement with the reported experimental data.<sup>[19,45]</sup> The nonpolar paraelectric cubic structure, space group *Pm $\bar{3}$ m*, becomes stable at temperatures higher than approximately 420 K.<sup>[46]</sup> Similarly to other perovskites,<sup>[20]</sup> this nonpolar phase can be stabilized at lower temperatures through light absorption, due to the presence of free carriers in the conduction band that screen the long-range dipole-dipole interactions sustaining ferroelectricity. This light-induced phase transition entirely is of electronic nature, as experimentally proven by Long and coworkers,<sup>[28]</sup> who verified that the temperature increase upon illumination is negligible. Therefore, it can be externally triggered within a vast temperature range spanning from absolute zero to  $T_c$ , as it has been recently discussed for KNbO<sub>3</sub>.<sup>[22,26]</sup>

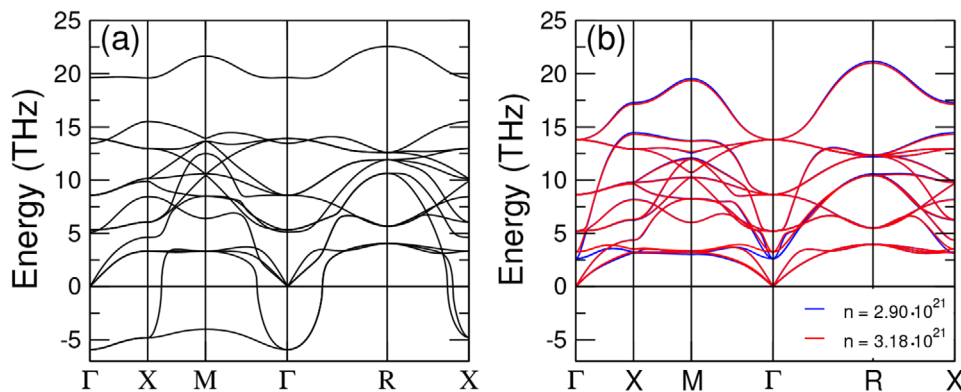


**Figure 1.** Phonon dispersion of cubic BTO under a) *dark* and b) *light* conditions for  $n \approx \bar{n} = 2.90 \cdot 10^{21} \text{ cm}^{-3}$  (blue line) and  $n = 3.18 \cdot 10^{21} \text{ cm}^{-3}$  (red line).

We found that the cubic phase of BTO can be stabilized by promoting an electron density  $n > \bar{n}$  to the conduction band, where  $\bar{n}$  is a threshold concentration that we estimate to be  $2.9 \cdot 10^{21} \text{ cm}^{-3}$ . This value is of the same order of the experimental estimate,<sup>[28]</sup> if one assumes that the photoexcited charge is concentrated near the surface.<sup>[47]</sup> **Figure 1** displays the zero-kelvin phonon dispersion calculated under *dark* conditions, featuring the well-known dynamical instability that drives the transition to the ferroelectric phase. In the same figure, we plot light-stabilized phonons, which now show stable dispersions without imaginary modes, for two different levels of charge injection. It is worth noting that, once the stabilization of the cubic phase is achieved, a further increase in  $n$  has an effect almost exclusively on the lowest-lying polar mode at  $\Gamma$  and the associated phonon band. Therefore, all the  $n$ -driven  $\kappa$  changes discussed below will be mostly caused by the character of this band, more specifically, its ability to participate in phonon-phonon scattering processes.

### 3.2. Photophononic Effects

We have computed the thermal conductivity of the light-stabilized cubic phase of BTO for six different values of the photoexcited charge,  $n$ ; notice that  $n$  indicates both the electron density in the conduction band and the hole density in the valence band, as all the investigated systems are charge neutral. Yet, we observe that similar effects can be obtained by impurity doping and charge transfer mechanisms, as long as mobile charge able to screen the long-range dipole-dipole interactions is present. As we are targeting a polar  $\rightarrow$  nonpolar (ferro-to-paraelectric in the case of BTO) phase transition at room temperature, all calculations –structural optimization, harmonic and anharmonic IFCs, solution of the BTE– have been carried out at the equilibrium volume obtained at 300 K within QHA (Section 2.1). Notice that, in the case of the light-stabilized cubic phase, the room-temperature equilibrium volume has been independently estimated for each value of  $n$ .

In **Figure 2** we plot the main results of our study: the absolute value of  $\kappa$  and its variation resulting from a polar  $\rightarrow$  nonpolar PIPT as a function of the density of photoexcited charge. As it can be appreciated, the thermal conductivity along the di-

rections perpendicular to the electric polarization,  $\kappa_{xx} = \kappa_{yy}$ , is considerably reduced at low photoexcited charge densities, being suppressed by as much as 30% for  $n \approx \bar{n}$ . This ratio increases, but it is always smaller than 1 (i.e., the thermal conductivity is reduced upon a polar  $\rightarrow$  nonpolar transition) for all the values of  $n$  considered. Things are different when considering heat flowing parallel to the electric polarization of the tetragonal phase,  $\kappa_{zz}$ . In this case, while for low photoexcited charge density the thermal conductivity is still reduced, at relatively low  $n$ 's, we found larger values for the nonpolar phase and thus the ferro-to-paraelectric PIPT results in an increase of  $\kappa_{zz}$ .

To note that the PIPT is accompanied by a considerable volume reduction ( $\Delta V/V = -2.5\%$  for  $n \approx \bar{n}$ , **Table 1**); thus, from a purely harmonic standpoint, one would expect an increase in  $\kappa$  due to

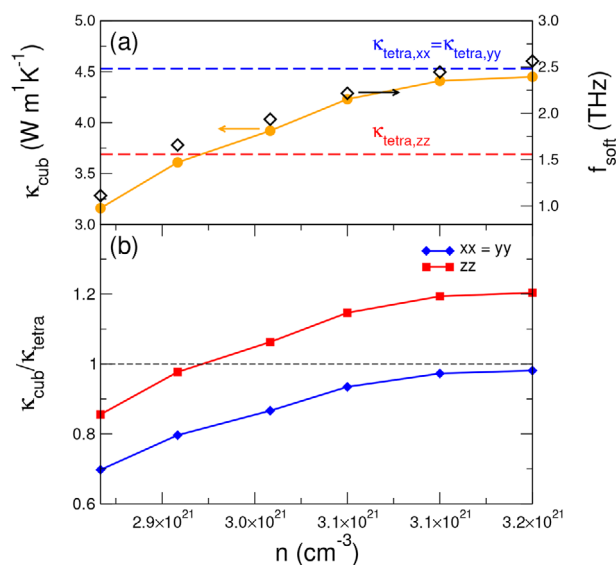


**Figure 2.** a) Thermal conductivity of the cubic phase and b) thermal conductivity change upon a polar-to-nonpolar PIPT as a function of  $n$ . The two independent elements of the thermal conductivity of the tetragonal phase (*dark* conditions) are indicated by dashed lines in the upper panel. The frequency at the  $\Gamma$  point of the soft mode,  $f_{\text{soft}}$ , as a function of  $n$  is indicated in the top panel (black diamonds).

**Table 1.** Lattice parameters and volume of the cubic phase under illumination for different photoexcited charge densities and of the tetragonal phase in dark conditions. All values have been estimated at 300 K within QHA.

$n[\times 10^{21} \text{ cm}^{-3}]$	a	c	$\bar{V} [\text{\AA}^3]$
Tetragonal			
–	4.003	4.010	65.700
Cubic			
2.90	4.008	–	64.362
2.95	4.006	–	64.292
3.01	4.006	–	64.279
3.06	4.005	–	64.246
3.12	4.005	–	64.224
3.18	4.004	–	64.211

the common hardening of the phonon modes and increase of phonon velocities (only in rare cases a decrease in  $\kappa$  accompanied by a volume reduction can be originated by anharmonic effects).<sup>[48]</sup> As observed in Figure 1b, the phonon dispersion of light-stabilized cubic phases obtained with different levels of excited charge only differ in the energy of the soft mode. Indeed, we found a remarkably strong correlation with the thermal conductivity variation, where low lying soft modes result in larger reductions of  $\kappa$  (Figure 2a), which evidences the crucial role played by the soft mode in optical control of the thermal conductivity in BTO.

Therefore, the observed behavior should be ascribable to anharmonic effects, almost entirely driven by role played by the soft mode. To corroborate this picture, we have computed the phonon lifetimes of the light-stabilized cubic phase,  $\tau_{\text{cub}}$ , and compared them to those of the *dark* tetragonal ground state,  $\tau_{\text{tetra}}$ . In Figure 3, we plot the quantity  $\Delta\tau = \tau_{\text{cub}} - \tau_{\text{tetra}}$ , obtained by averaging the lifetimes within frequency intervals of 0.25 THz, for three different values of  $n$ . In the case of low charge injection ( $\bar{n} = 2.90 \cdot 10^{21} \text{ cm}^{-3}$ , the threshold value to stabilize the cubic phase),  $\Delta\tau$  is negative throughout the entire frequency range, indicating that phonons in the nonpolar phase always have shorter lifetimes than in the polar phase, which accounts for the considerable reduction in the thermal conductivity reported in Figure 2. For the higher photoexcited charge  $n = 3.01 \cdot 10^{21} \text{ cm}^{-3}$ ,  $\Delta\tau$  is still negative in all the considered frequency range; however its absolute value is smaller, particularly for heat-carrying, low-frequency phonons. This behavior is consistent with the results obtained for  $\kappa$ , which reduces upon the polar  $\rightarrow$  nonpolar phase transition but in a smaller amount than for  $n \approx \bar{n}$ . Finally, at the highest considered charge excitation,  $n = 3.18 \cdot 10^{21} \text{ cm}^{-3}$ , the case is quite different since at low frequencies we observe an inversion of the trend and the phonons in the nonpolar phase are longer-lived than those in the polar phase. Indeed, for this value of the photoexcited charge we found that  $\kappa_{zz}$  is  $\approx 20\%$  larger in the cubic phase, while the thermal conductivity in the plane perpendicular to the electric polarization axis of the tetragonal phase,  $\kappa_{xx} = \kappa_{yy}$ , is essentially unchanged (i.e.,  $\mathbf{P}$  is parallel to the z-axis).

The  $\kappa$  behavior found in the highest photoexcitation regime can be easily understood by looking at the upper panel of Figure 2, where the value of  $\kappa_{\text{cub}}$  is displayed. As can be seen there, at large  $n$ , the thermal conductivity of the nonpolar phase

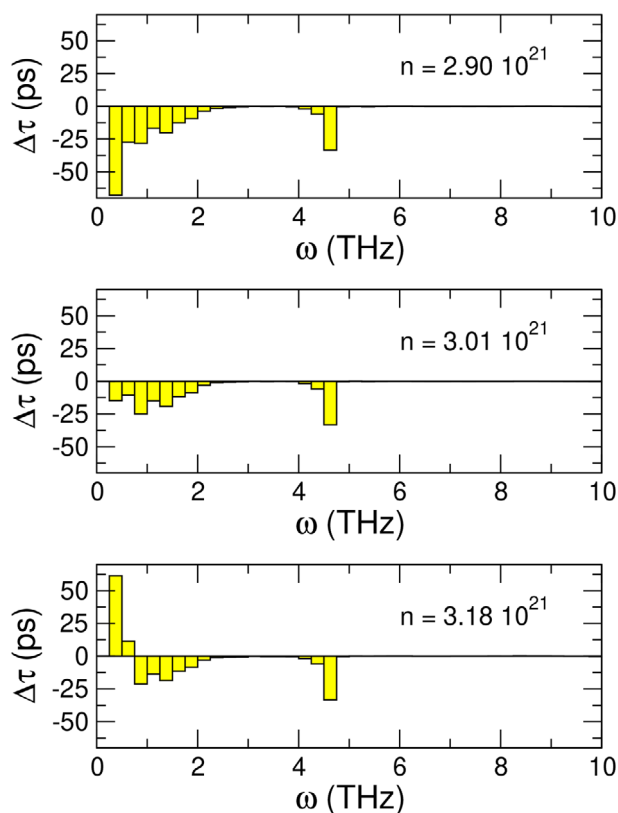


**Figure 3.** Difference between the lifetimes in the cubic and tetragonal phase averaged over frequency intervals of 0.25 THz for different values of the photoexcited charge ( $n = 2.90 \cdot 10^{21}$ ,  $3.01 \cdot 10^{21}$ , and  $3.18 \cdot 10^{21} \text{ cm}^{-3}$ , top to bottom).

approaches the value of  $\kappa_{xx} = \kappa_{yy}$  of the tetragonal phase. This is not surprising, as the  $x$ - and  $y$ -axis are precisely the directions along which there is no polar distortion. Interestingly, as  $n$  increases, the lattice constant of the cubic phase also tends to the value of the lattice parameter of tetragonal phase along the short axis,  $a$  (Table 1).

It should be noted that, once a finite photoexcited charge density is present, the electronic contribution to the thermal conductivity,  $\kappa_{\text{el}}$ , can no longer be neglected outright, as customary in semiconductors and insulators. For this reason, we have used the electron–phonon averaged approximation (EPA)<sup>[49]</sup> in combination with BoltzTraP2<sup>[50]</sup> to compute  $\kappa_{\text{el}}$  of the light-stabilized cubic phase. We found values that are order of magnitudes lower than those of the lattice counterpart of  $\kappa$  discussed thus far across a range of temperatures (see the Supporting Information). This clearly suggests that the change in thermal conductivity upon the polar  $\rightarrow$  nonpolar phase transition discussed here is governed by phonons and that electronic contribution can be safely neglected.

### 3.3. Light- versus Temperature-Stabilized Cubic Phase

The Curie temperature,  $T_c$ , of BTO is 420 K<sup>[46]</sup> and for  $T > T_c$  the crystal structure is cubic. It is thus interesting to compare the phononic properties of such high temperature cubic phase with the light-stabilized cubic phase that we have analyzed in

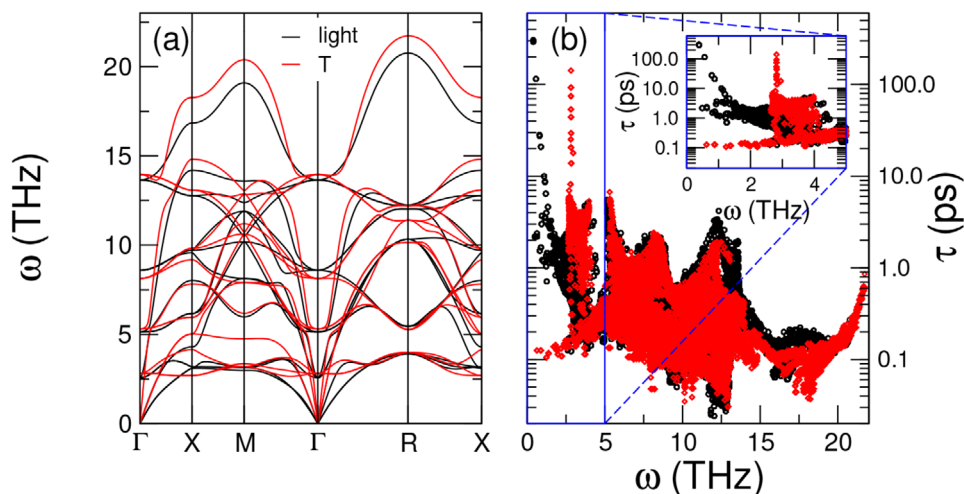


**Figure 4.** a) Phonon dispersion and b) phonon lifetimes of a light- and a temperature-stabilized cubic phase, in black and red, respectively. The inset displays a zoomed view of the lifetimes of low frequency phonons.

Sections 3.1 and 3.2. In the first case the cubic structure is stabilized by a lattice-dynamical effect, while in the second case the stabilization has a purely electronic origin.

In order to compare cases that are as similar as possible, we consider a temperature-stabilized cubic phase at 300 K. At this temperature,  $T < T_c$ , the ground state is still the ferroelectric one. Yet, the cubic phase is predicted to be metastable and the renormalization procedure to compute finite temperature phonons leads to a well-behaved dispersion (i.e., without imaginary modes), allowing for the calculation of the thermal conductivity. On the other hand, in the light-stabilized case we proceed as described above: we rely on zero-kelvin phonons and stabilize the cubic phase by means of photoexcited charge. Notice that the observed room temperature dynamical stability of the cubic phase) implies that the widely used “two-well displacive model” should be handled with care, as it is most appropriate for second-order (continuous) transitions, where the order parameter vanishes smoothly at the critical temperature. However, our results corroborate experimental studies, which report strong electrocaloric effects, indicating that BTO rather undergoes a first-order phase transition.<sup>[51,52]</sup>

According to the results shown in Figure 2, when  $n$  is larger than  $\approx 3.1 \times 10^{21} \text{ cm}^{-3}$ ,  $\kappa$  approaches a saturation value of  $\approx 4.5 \text{ W m}^{-1} \text{ K}^{-1}$ . Hence, we take the case of  $n = 3.18 \times 10^{21} \text{ cm}^{-3}$  as a prototypical light-stabilized cubic phase and compare its phonon dispersion, phonon lifetimes and thermal conductivity with those of a cubic phase stabilized by temperature.

First, we notice that we obtain slightly different equilibrium volumes,  $\bar{V}$ , at 300 K. Independent estimates based on QHA lead to  $\bar{V} = 64.2 \text{ \AA}^3$  and  $63.9 \text{ \AA}^3$  for the light- and temperature-stabilized phases, respectively, indicating a non-negligible photoinduced electronic pressure<sup>[20,41]</sup> in the first case (see also Table 1 for the evolution of  $\bar{V}$  as a function of  $n$ ). Accordingly, we found higher phonon frequencies for the temperature-stabilized cubic phase, due to the a smaller  $\bar{V}$  (Figure 4a). The resulting higher acoustic phonon velocities alone would lead to a larger  $\kappa$  compared to the light-stabilized case.

The situation is completely different when one looks at anharmonic properties, as shown in Figure 4b. The lifetimes of the light-stabilized cubic phase are larger, particularly when it comes to low frequency phonons, which usually carry the larger fraction of the total heat flux. In particular, as shown in the inset of the same figure, we found an almost complete suppression of phonons with  $\omega < 2.5 \text{ THz}$  for the temperature-stabilized phase. In that frequency range, the corresponding  $\tau$ 's are 2 to 4 orders of magnitude lower than those of the light-stabilized case.

Similar competing effects were encountered in Section 3.2, where analysis solely based on harmonic (anharmonic) properties would lead to a larger  $\kappa$  of the nonpolar (polar) phase. Also in this case, we found that the overall behavior is dictated by phonon–phonon anharmonic scattering and that the shorter lifetimes of low frequency phonons of the temperature-stabilized phased overcompensate the higher phonon velocities, leading to a computed thermal conductivity of  $3.25 \text{ W m}^{-1} \text{ K}^{-1}$  (to be compared with  $4.60 \text{ W m}^{-1} \text{ K}^{-1}$  of the light-stabilized cubic phase).

Of note is that, only for the lowest photoexcited charge density, one is able to find a  $\kappa$  of the light-stabilized phase as low as the one of the temperature-stabilized phase (Figure 2). For all the other values of  $n$ , we found an anharmonic-driven reduction of  $\kappa$  of the temperature- as compared to the light-stabilized cubic phase (see the Supporting Information for the plots of the phonon dispersion and lifetime at each  $n$ ).

## 4. Conclusion

In summary, our study demonstrates that light-driven manipulation of thermal conductivity in ferroelectric BTO offers a novel and effective approach for dynamic thermal control, circumventing the limitations of static modifications like doping and structural defects. Through first-principles simulations, we reveal that photoinduced charge excitation induces a reversible ferro-to-paraelectric phase transition in BTO, yielding substantial reductions in lattice thermal conductivity. This effect is particularly pronounced at low levels of photoexcited charge density, where we observe a marked suppression of the low-frequency

phonon modes, a critical factor in limiting heat flow. These findings highlight the pivotal role of phonon-phonon scattering in enabling real-time control over thermal properties under light excitation, which is unattainable through conventional thermal management methods.

It is important to stress that PIPTs like the one studied here have already been reported experimentally. Beside the experiments on BTO,<sup>[27–29]</sup> already discussed and of special relevance for our work, other PIPTs have been demonstrated. Krapivin and coworkers<sup>[53]</sup> have reported a light-induced suppression of the ferroelectric instability in  $\text{KTaO}_3$ . Similarly, Guo and coworkers<sup>[54]</sup> very recently demonstrated the ultrafast lattice manipulation of ferroelectric  $\text{In}_2\text{Se}_3$ , where different phase transitions can be triggered by means of femtosecond laser pulses. Photoexcitation can also be used to affect other types of charge ordering, such as charge density waves; light-induced melting of the CDW has been reported in  $\text{TiSe}_2$ ,<sup>[23,24]</sup> while a transformation between the 2H and 1T polymorphs of  $\text{MoTe}_2$  has been predicted theoretically.<sup>[21]</sup> Yet, studies on how such light-induced phase transformations can affect the thermal transport properties of materials are still very scarce.

The significance of this work extends beyond BTO, as it suggests that light-induced phase transitions could be harnessed in other polar materials to achieve tunable thermal conductivity. Other ferroelectric perovskites that are good candidates to observe similar effects are those whose ferroelectric instability depends strongly on the action of dipole-dipole electrostatic couplings, susceptible to be screened (weakened) upon photoexcitation.<sup>[20,55]</sup> Such materials include  $\text{NaNbO}_3$  and possibly solid solutions based on  $\text{BaTiO}_3$  and  $\text{KNbO}_3$  (though in this case the role of elastic scattering, which can potentially hinder these effects, should be addressed). We can also expect more subtle structural phase transitions in other ferroelectric perovskites, e.g., solid solutions based on  $\text{PbTiO}_3$ .<sup>[20]</sup> Note that theoretical predictions of a sizeable photophononic effect in  $\text{KNbO}_3$  have already been presented,<sup>[22]</sup> while archetypal ferroelectric perovskite  $\text{PbTiO}_3$  cannot be stabilized by photoexcitation.<sup>[20]</sup> This reversible, ultrafast control presents exciting opportunities for applications ranging from adaptive microelectronic cooling systems to energy-efficient thermoelectric devices. By establishing a basis for photophononic effects in thermal management, our findings underscore the potential of photoactive materials in advancing smart and sustainable technologies.

## Supporting Information

Supporting Information is available from the Wiley Online Library or from the author.

## Acknowledgements

The authors thank Ignasi Fina for useful discussions about their experiments. The authors acknowledge financial support by MCIN/AEI/10.13039/501100011033 under grant PID2020-119777GB-I00, TED2021-130265B-C22, PID2020-112975GB-I00, the “Ramón y Cajal” fellowship RYC2018-024947-I and the Severo Ochoa Centres of Excellence Program under grant CEX2023-001263-S, and by the Generalitat de Catalunya under grants 2021 SGR 01519 and 2021 SGR 00343. The authors thank the Centro de Supercomputación de Galicia (CESGA)

for the use of their computational resources. Work at LIST was supported by the Luxembourg National Research Fund through Grant C21/MS/15799044/FERRODYNAMICS.

## Conflict of Interest

The authors declare no conflict of interest.

## Data Availability Statement

The data that support the findings of this study are available from the corresponding author upon reasonable request.

## Keywords

$\text{BaTiO}_3$ , ferroelectrics, phonons, photoinduced phase transition, thermal conductivity

Received: December 23, 2024

Revised: May 23, 2025

Published online:

- [1] E. Pop, *Nano Res.* **2010**, *3*, 147.
- [2] M. Zebarjadi, K. Esfarjani, M. S. Dresselhaus, Z. F. Ren, G. Chen, *Energy Environ. Sci.* **2012**, *5*, 5147.
- [3] A. L. Moore, L. Shi, *Mater. Today* **2014**, *17*, 163.
- [4] G. Benenti, G. Casati, K. Saito, R. S. Whitney, *Phys. Rep.* **2017**, *694*, 1.
- [5] I. Zardo, R. Rurali, *Curr. Opin. Green Sustain. Chem.* **2019**, *17*, 1.
- [6] C. Cazorla, M. Stengel, J. Íñiguez, R. Rurali, *npj Comput. Mater.* **2023**, *9*, 97.
- [7] C. Liu, Y. Si, H. Zhang, C. Wu, S. Deng, Y. Dong, Y. Li, M. Zhuo, N. Fan, B. Xu, P. Lu, L. Zhang, X. Lin, X. Liu, J. Yang, Z. Luo, S. Das, L. Bellaiche, Y. Chen, Z. Chen, *Science* **2023**, *382*, 1265.
- [8] C. Cazorla, R. Rurali, *Phys. Rev. B* **2022**, *105*, 104401.
- [9] G. F. Nataf, S. Volz, J. Ordonez-Miranda, J. Íñiguez González, R. Rurali, B. Dkhil, *Nat. Rev. Mater.* **2024**, *9*, 530.
- [10] J. F. Ihlefeld, B. M. Foley, D. A. Scrymgeour, J. R. Michael, B. B. McKenzie, D. L. Medlin, M. Wallace, S. Trolier-McKinstry, P. E. Hopkins, *Nano Lett.* **2015**, *15*, 1791.
- [11] J. A. Seijas-Bellido, C. Escorihuela-Salayero, M. Royo, M. P. Ljungberg, J. C. Wojdeł, J. Íñiguez, R. Rurali, *Phys. Rev. B* **2017**, *96*, 140101(R).
- [12] M. Royo, C. Escorihuela-Salayero, J. Íñiguez, R. Rurali, *Phys. Rev. Mater.* **2017**, *1*, 051402(R).
- [13] C. Liu, Y. Chen, C. Dames, *Phys. Rev. Appl.* **2019**, *11*, 044002.
- [14] E. Langenberg, D. Saha, M. E. Holtz, J.-J. Wang, D. Bugallo, E. Ferreiro-Vila, H. Paik, I. Hanke, S. Ganschow, D. A. Muller, L.-Q. Chen, G. Catalan, N. Domingo, J. Malen, D. G. Schlom, F. Rivadulla, *Nano Lett.* **2019**, *19*, 7901.
- [15] P. Torres, J. A. Seijas-Bellido, C. Escorihuela-Salayero, J. Íñiguez, R. Rurali, *Phys. Rev. Materials* **2019**, *3*, 044404.
- [16] J. A. Seijas-Bellido, H. Aramberrí, J. Íñiguez, R. Rurali, *Phys. Rev. B* **2018**, *97*, 184306.
- [17] J. A. Seijas-Bellido, i. J. Íñiguez, R. Rurali, *Appl. Phys. Lett.* **2019**, *115*, 192903.
- [18] P. Torres, J. Íñiguez, R. Rurali, *Phys. Rev. Lett.* **2019**, *123*, 185901.
- [19] L. Féger, C. Escorihuela-Salayero, J.-M. Rampnoux, K. Kontou, M. Bah, J. Íñiguez González, C. Cazorla, I. Monot-Laffez, S. Douri, S. Grauby, R. Rurali, S. Dilhaire, S. Gomès, G. F. Nataf, *Phys. Rev. Mater.* **2024**, *8*, 094403.

- [20] C. Paillard, E. Torun, L. Wirtz, J. Íñiguez, L. Bellaiche, *Phys. Rev. Lett.* **2019**, 123, 087601.
- [21] B. Peng, Y. Hu, S. Murakami, T. Zhang, B. Monserrat, *Sci. Adv.* **2020**, 6, eabd1618.
- [22] C. Cazorla, S. Bichelmaier, C. Escorihuela-Sayalero, J. Íñiguez, J. Carrete, R. Rurali, *Nanoscale* **2024**, 16, 8335.
- [23] E. Möhr-Vorobeva, S. L. Johnson, P. Beaud, U. Staub, R. D. Souza, C. M. G. Ingold, J. Demsar, H. Schaefer, A. Titov, *Phys. Rev. Lett.* **2011**, 107, 036403.
- [24] M. Huber, Y. Lin, G. Marini, L. Moreschini, C. Jozwiak, A. Bostwick, M. Calandra, A. Lanzara, *Sci. Adv.* **2024**, 10, ead14481.
- [25] M. Raya-Moreno, C. Cazorla, E. Canadell, R. Rurali, *npj 2D Mater. Appl.* **2024**, 8, 64.
- [26] R. Rurali, C. Escorihuela-Sayalero, J. L. Tamarit, J. Íñiguez González, C. Cazorla, *Phys. Rev. Lett.* **2024**, 133, 116401.
- [27] X. Long, H. Tan, F. Sánchez, I. Fina, J. Fontcuberta, *Nat. Commun.* **2021**, 12, 382.
- [28] X. Long, H. Tan, F. Sánchez, I. Fina, J. Fontcuberta, *J. Appl. Phys.* **2022**, 132, 214103.
- [29] H. Tan, G. Castro, J. Lyu, P. Loza-Alvarez, F. Sánchez, J. Fontcuberta, I. Fina, *Mater. Horiz.* **2022**, 9, 2345.
- [30] G. Kresse, J. Hafner, *Phys. Rev. B* **1993**, 47, 558.
- [31] G. Kresse, J. Hafner, *Phys. Rev. B* **1994**, 49, 14251.
- [32] G. Kresse, D. Joubert, *Phys. Rev. B* **1999**, 59, 1758.
- [33] P. E. Blöchl, *Phys. Rev. B* **1994**, 50, 17953.
- [34] J. P. Perdew, A. Ruzsinszky, G. I. Csonka, O. A. Vydrov, G. E. Scuseria, L. A. Constantin, X. Zhou, K. Burke, *Phys. Rev. Lett.* **2008**, 100, 136406.
- [35] A. Togo, L. Chaput, I. Tanaka, *Phys. Rev. B* **2015**, 91, 094306.
- [36] A. Carreras, A. Togo, I. Tanaka, *Comput. Phys. Commun.* **2017**, 221, 221.
- [37] W. Li, J. Carrete, N. A. Katcho, N. Mingo, *Comp. Phys. Commun.* **2014**, 185, 1747.
- [38] J. Carrete, B. Vermeersch, A. Katre, A. van Roekeghem, T. Wang, G. K. Madsen, N. Mingo, *Comput. Phys. Commun.* **2017**, 220, 351.
- [39] C. Cazorla, D. Errandonea, E. Sola, *Phys. Rev. B* **2009**, 80, 064105.
- [40] C. Cazorla, J. Boronat, *Rev. Mod. Phys.* **2017**, 89, 035003.
- [41] C. Paillard, S. Prosandeev, L. Bellaiche, *Phys. Rev. B* **2017**, 96, 045205.
- [42] L. Hedin, *Phys. Rev.* **1965**, 139, A796.
- [43] M. Marques, E. Gross, *Annu. Rev. Phys. Chem.* **2004**, 55, 427.
- [44] B. Peng, H. Zhang, W. Chen, B. Hou, Z.-J. Qiu, H. Shao, H. Zhu, B. Monserrat, D. Fu, H. Weng, C. M. Soukoulis, *npj 2D Mater. Appl.* **2020**, 4, 14.
- [45] B. Jaffe, W. Cook, H. Jaffe, (Eds), *Piezoelectric Ceramics*, Academic Press, Inc., London, UK **1971**.
- [46] M. Harwood, P. Popper, D. Rushman, *Nature* **1947**, 160, 58.
- [47] Y. V. Podgorny, K. A. Vorotilov, A. S. Sigov, J. F. Scott, *Appl. Phys. Lett.* **2019**, 114, 132902.
- [48] Y. Zhou, Z.-Y. Dong, W.-P. Hsieh, A. F. Goncharov, X.-J. Chen, *Nat. Rev. Phys.* **2022**, 4, 319.
- [49] G. Samsonidze, B. Kozinsky, *Adv. Energy Mater.* **2018**, 8, 1800246.
- [50] G. K. Madsen, J. Carrete, M. J. Verstraete, *Comput. Phys. Commun.* **2018**, 237, 140.
- [51] X. Moya, E. Stern-Taulats, S. Crossley, D. González-Alonso, S. Kar-Narayan, A. Planes, L. Mañosa, N. D. Mathur, *Adv. Mater.* **2013**, 25, 1360.
- [52] J. Li, A. Torelló, Y. Nouchokgwe, T. Granzow, V. Kovacova, S. Hirose, E. Defay, *J. Phys.: Energy* **2023**, 5, 024017.
- [53] V. Krapivin, M. Gu, D. Hickox-Young, S. W. Teitelbaum, Y. Huang, G. de la Peña, D. Zhu, N. Sirica, M.-C. Lee, R. P. Prasankumar, A. A. Maznev, K. A. Nelson, M. Chollet, J. M. Rondinelli, D. A. Reis, M. Trigo, *Phys. Rev. Lett.* **2022**, 129, 127601.
- [54] J. Guo, L. Zhang, M. Zhang, S. Ji, Z. Xiao, C. Gao, F. Liu, Z. Hu, Y. Zhou, X. Fu, *ACS Nano* **2025**, 19, 13264.
- [55] H. J. Zhao, A. Filippetti, C. Escorihuela-Sayalero, P. Delugas, E. Canadell, L. Bellaiche, V. Fiorentini, J. Íñiguez, *Phys. Rev. B* **2018**, 97, 054107.